Journal of Power Sources 188 (2009) 38–44

Contents lists available at ScienceDirect

Journal of Power Sources

journal homepage: www.elsevier.com/locate/jpowsour

Nitrogen-modified carbon-based catalysts for oxygen reduction reaction in polymer electrolyte membrane fuel cells

Nalini P. Subramanian, Xuguang Li, Vijayadurda Nallathambi, Swaminatha P. Kumaraguru, Hector Colon-Mercado, Gang Wu, Jong-Won Lee, Branko N. Popov*

Center for Electrochemical Engineering, Department of Chemical Engineering, University of South Carolina, Columbia, SC 29208, USA

ARTICLE INFO

Article history:
Received 2 October 2008
Received in revised form
21 November 2008
Accepted 24 November 2008
Available online 28 November 2008

Keywords:
Carbon-based catalyst
Nitrogen modification
Oxygen reduction
PEM fuel cell

ABSTRACT

Nitrogen-modified carbon-based catalysts for oxygen reduction were synthesized by modifying carbon black with nitrogen-containing organic precursors. The electrocatalytic properties of catalysts were studied as a function of surface pre-treatments, nitrogen and oxygen concentrations, and heat-treatment temperatures. On the optimum catalyst, the onset potential for oxygen reduction is approximately 0.76 V (NHE) and the amount of hydrogen peroxide produced at 0.5 V (NHE) is approximately 3% under our experimental conditions. The characterization studies indicated that pyridinic and graphitic (quaternary) nitrogens may act as active sites of catalysts for oxygen reduction reaction. In particular, pyridinic nitrogen, which possesses one lone pair of electrons in addition to the one electron donated to the conjugated π bond, facilitates the reductive oxygen adsorption.

© 2008 Elsevier B.V. All rights reserved.

1. Introduction

Platinum (Pt) is the most commonly used electrocatalyst for the four-electron oxygen reduction to water in acidic environments with low overpotential and high stability [1–5]. However, even on pure Pt, the overpotential caused by sluggish kinetics is in excess of 300 mV (NHE) from the thermodynamic potential for oxygen reduction reaction (ORR). Furthermore, due to the high cost and limited availability of Pt, it is of great interest to find low-cost non-precious metal alternatives.

Since Jasinski's discovery of the catalytic properties of Co phthalocyanines [6], there has been a considerable research on non-precious metal catalysts such as: (i) transition metal macrocyclic compounds (e.g., cobalt phthalocyanines and iron tetramethoxyphenyl porphyrin) [7–23], (ii) vacuum-deposited cobalt and iron compounds (e.g., Co–C–N and Fe–C–N) [24,25], and (iii) metal carbides, nitrides and oxides (e.g., FeC_x, TaO_xN_y, MnO_x/C) [26,27]. However, the nature of the active sites of these catalysts for oxygen reduction is still an open question.

The most commonly accepted hypothesis and the relevant reaction mechanism of oxygen reduction on non-precious metal catalysts is that the metal–N_4 moiety bound to the carbon support plays a crucial role in the oxygen reduction reaction [7–23]. However, Yeager [28] and Wiesener [29] suggested that the transition metal does not act as an active reaction site for oxygen reduction, but rather serves primarily to facilitate the stable incorporation of nitrogen into the graphitic structure during high-temperature pyrolysis of metal–nitrogen complexes. According to Maldonado and Stevenson [30] the strong basicity of N-doped carbons facilitates reductive O_2 adsorption and the decomposition of peroxide species, thereby increasing the catalytic activity. This idea is strongly supported by our experimental findings on CoN/C-based catalysts [31–37]. X-ray photoelectron spectroscopy (XPS) data indicated that the pyrolysis in the presence of Co increases the concentrations of two nitrogen functional groups on the carbon surfaces (pyridinic-type nitrogen and quaternary carbon-graphitic-type nitrogen). The subsequent dissolving out of Co metals from the heat-treated Co–N chelates does not cause any loss of the catalytic activity; instead, the catalytic activity increased by removing the excess un-active Co species and thus the exposure of true active sites.

Nitrogen-containing carbon catalysts can be prepared using implantation, through NH_3 or HCN treatment of an oxidized carbon. The electrochemical measurements in our laboratory indicated that onset potential of oxygen reduction on the NH_3-treated Ketjen black is approximately 0.5 V (NHE) in comparison with 0.3 V (NHE) on the untreated carbon [31]. The quantum mechanical calculations on cluster models show that carbon radical sites formed adjacent to substitutional N in the NH_3-treated carbon are active sites for ORR [38]. Matter et al. [39–41] prepared an active non-metal catalyst for oxygen reduction by the decomposition of acetonitrile vapor at 900 °C over a pure alumina support and an alumina sup-

* Corresponding author. Tel.: +1 803 777 7314; fax: +1 803 777 8265.
E-mail address: popov@engr.sc.edu (B.N. Popov).

0378-7753/$ – see front matter © 2008 Elsevier B.V. All rights reserved.
doi:10.1016/j.jpowsour.2008.11.087

port containing 2 wt% Fe or 2 wt% Ni. The catalysts showed only 100 mV (NHE) greater overpotential than Pt catalyst for oxygen reduction. The authors also studied the role of nanostructure playing in nitrogen-containing carbon catalyst for oxygen reduction. The most active catalyst was obtained when Fe-containing alumina support is used. The activity of catalysts was attributed to significantly high amount of pyridinic nitrogen.

In this work, the nitrogen-modified carbon-based catalyst was prepared by oxidizing carbon black with nitric acid followed by chemical modification with nitrogen-rich precursors such as melamine, urea, thiourea, and selenourea. Rotating ring-disk electrode (RRDE) technique was performed to evaluate the activity and selectivity of catalysts. The nature of the active sites of catalysts was discussed based on various physical and chemical characterizations.

2. Experimental

2.1. Catalyst synthesis

Nitrogen-modified carbon-based catalysts were prepared with a four-step process that includes (i) removal of metal impurities, (ii) chemical oxidation of carbon support, (iii) synthesis of nitrogen-rich polymeric resins on the oxidized carbon, and (iv) pyrolysis of the resulting powder at elevated temperatures in an inert atmosphere.

Initially, commercially available Ketjen Black EC 300J was pre-washed with 6 M HCl to remove any of metal impurities on the carbon. The carbon was washed several times with deionized water to remove any of chloride and metal impurities. The pre-washed carbon was subject to oxidation in 70% HNO_3 for 7 h under refluxing conditions and then washed in distilled water followed by drying in an oven at 75 °C.

Various nitrogen-based resins such as melamine formaldehyde (MF), urea formaldehyde (UF), thiourea formaldehyde (TUF), and selenourea formaldehyde (SeUF) were synthesized by a simple addition–condensation reaction on the oxidized carbon [42]. In the first step, by the addition of formaldehyde, melamine or urea is hydroxymethylolated to the amino groups. In the case of UF, this reaction leads to the formation of mono-, di- and tri-metalylureas. The second step consists of condensation of the methylolureas to low molecular weight polymers. The condensation reaction occurs only at acidic environment and results in the formation of methylene bridges between amido nitrogens and methylene ether linkages by the reaction of two methylol groups.

For every 10 g of the oxidized carbon black, melamine, urea, thiourea or selenourea was mixed with formaldehyde in 100 ml of distilled water. The molar ratio of melamine to formaldehyde in the precursor solution was maintained at 1:3, and the urea (or thiourea, selenourea) to formaldehyde was 1:2. After the solution temperature reaches 50 °C, NaOH solution was added to bring the pH of the solution to around 10.0. This initiates the addition reaction. Then, the polymerization reaction was initiated by increasing the temperature of the solution to 75 °C and by acidifying the solution with H_2SO_4 solution to pH 2.5. The solution was stirred for 4 h. The resulting gel was dried overnight in a vacuum oven at 90 °C. The resulting powder was placed in a quartz boat and inserted into a 10 cm diameter quartz tube. The pyrolysis was carried out at high temperatures in the range of 400–1000 °C for 90 min. N_2 gas was purged into the reactor continuously throughout the pyrolysis step.

2.2. Electrochemical characterization

Electrochemical characterization of the synthesized catalysts was performed in a rotating ring-disk electrode setup that employs a standard three-compartment electrochemical cell. The RRDE has a platinum ring (5.52 mm inner diameter and 7.16 mm outer diameter) and a glassy carbon disk (5.0 mm diameter) as the working electrode; a saturated mercury–mercury sulfate electrode is the reference electrode and a platinum foil acts as the counter electrode. All potentials in this work were referred to a normal hydrogen electrode (NHE).

The catalyst ink was prepared by ultrasonically blending 8 mg of catalyst with 1 mL of isopropyl alcohol. 15 μL of the ink was then deposited onto the glassy carbon surface. 5 μL of 0.25 wt% Nafion solution (a mixture of 5 wt% Nafion solution and isopropyl alcohol with the volume ratio of 1:19) was applied onto catalyst layer to ensure better adhesion of catalyst onto glassy carbon. 0.5 M H_2SO_4 was the electrolyte. The system was purged with N_2 to clean the surface of catalyst by scanning the potential between 1.04 and 0.04 V (NHE) at a sweep rate of 50 mV s^{-1}. The electrode was scanned in N_2 saturated electrolyte at a sweep rate of 5 mV s^{-1} to evaluate the background capacitance current. The electrocatalytic activity of catalyst was then measured by saturating the electrolyte with O_2. Linear sweep voltammograms were measured at 900 rpm. The ring potential was maintained at 1.2 V (NHE) throughout the experiment in order to oxidize H_2O_2 produced during oxygen reduction on disk electrode. The percentage of H_2O_2 was calculated using the following equation:

$$\%H_2O_2 = \frac{200(I_r/N)}{I_d + (I_r/N)} \quad (1)$$

where I_d, I_r and N are the disk current, ring current and collection efficiency, respectively. The value of N was taken as 0.39 for our experiments.

2.3. Fuel cell testing

To construct the membrane-electrode assemblies (MEAs), the cathode catalyst ink was prepared by ultrasonically blending catalyst with Nafion solution and isopropyl alcohol for 4 h. The catalyst ink was then sprayed onto a gas diffusion layer (GDL) (ELAT LT 1400W, E-TEK) until a desired catalyst loading has been achieved. A commercially catalyzed GDL (0.5 mg cm^{-2} Pt, E-TEK) was used as the anode. A thin layer of Nafion was coated on both the cathode and anode surfaces. The Nafion-coated anode and cathode were hot-pressed to a Nafion 112 membrane at 140 °C and 534 kPa for 3 min. The geometric area of the electrode was 5 cm^2.

The MEA testing was carried out in a single cell with serpentine flow channels. Pure H_2 gas humidified at 77 °C and pure O_2 gas humidified at 75 °C were supplied to the anode and cathode compartments, respectively. The measurements were conducted using a fully automated test station (Fuel Cell Technologies Inc.) at 75 °C. In order to evaluate the durability of the catalyst, potentiostatic current transient technique was used by applying a constant potential of 0.4 V.

2.4. Physical and chemical characterizations

Surface analysis of the catalyst was performed using X-ray photoelectron spectroscopy (XPS) with a KRATOS AXIS 165 high performance electron spectrometer. Inductively coupled plasma-mass spectroscopy (ICP-MS) was conducted with an SCIEX ELAN DRCe ICP-MS system (PerkinElmer) to analyze the bulk transition metals in the catalysts. X-ray diffraction (XRD) pattern was recorded on an automated Rigaku diffractometer equipped with a Cu Kα radiation and a graphite monochromatic operation at 45 kV and 40 mA. Transmission electron microscopy (TEM, Hitachi H-8000) was used to determine the distribution of carbon and to confirm the absence of metal particles in the catalyst. The BET surface area of the catalyst

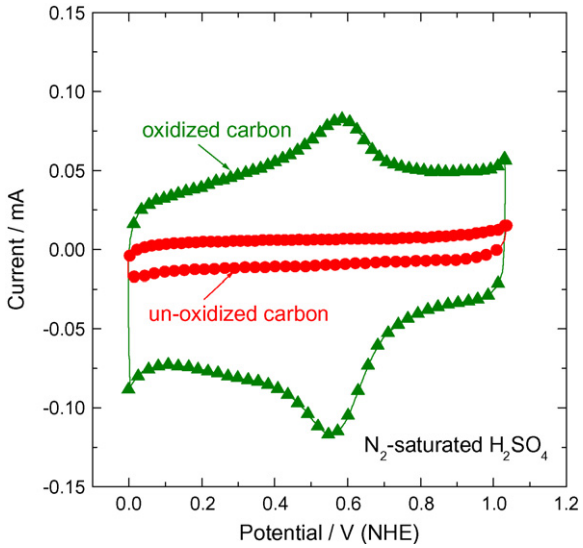

Fig. 1. Cyclic voltammograms of the un-oxidized and oxidized carbons. The measurements were performed in N_2 saturated 0.5 M H_2SO_4 solution using a potential scan rate of 5 mV s^{-1}.

was evaluated in a Quantachrome NOVA BET 2000 analyzer using N_2 gas sorption.

3. Results and discussion

3.1. Electrochemical, physical and chemical studies of carbon-based catalysts modified with different nitrogen donors

Fig. 1 shows the cyclic voltammograms of the un-oxidized and oxidized carbons. The measurements were performed in N_2 saturated 0.5 M H_2SO_4 solution at a potential scan rate of 5 mV s^{-1}. In comparison with the un-oxidized carbon, the oxidized carbon exhibits well-defined redox peaks at about 0.55 V (NHE). These characteristic peaks are associated with the quinine–hydroquinone redox couple [43].

Fig. 2 shows the polarization curves of oxygen reduction on the un-oxidized and oxidized carbons. The RRDE measurements were performed in O_2 saturated 0.5 M H_2SO_4 solution at a potential scan rate of 5 mV s^{-1} and a rotation speed of 900 rpm. The un-oxidized carbon exhibited very low activity for oxygen reduction. With the introduction of oxygen-containing groups on carbon surface by HNO_3 treatment, the activity of carbon black for oxygen reduction increases. This is attributed to the presence of quinone type groups [43–45].

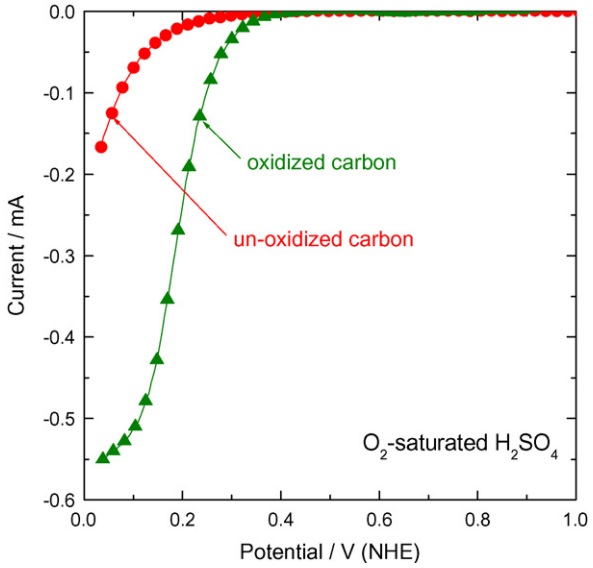

Fig. 2. Polarization curves of oxygen reduction on the un-oxidized and oxidized carbons. The measurements were performed in O_2 saturated 0.5 M H_2SO_4 solution using a potential scan rate of 5 mV s^{-1} and a rotation speed of 900 rpm.

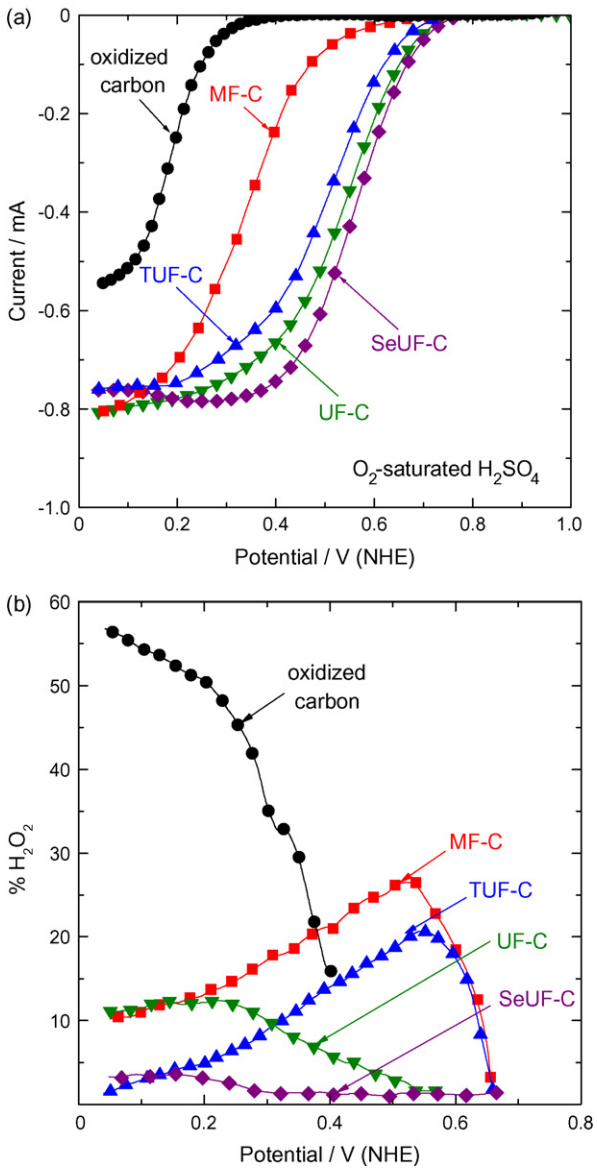

Fig. 3. (a) Polarization curves of oxygen reduction and (b) percentages of H_2O_2 formed during oxygen reduction on carbon-based catalysts modified with different nitrogen donors and heat-treated at 800 °C. For comparison, the curve measured on the oxidized carbon was also shown. The measurements were performed in O_2 saturated 0.5 M H_2SO_4 solution using a potential scan rate of 5 mV s^{-1} and a rotation speed of 900 rpm.

Fig. 3 shows the polarization curves of oxygen reduction on carbon-based catalysts modified with different nitrogen donors and heat-treated at 800 °C. It was observed that the onset potential of oxygen reduction on melamine formaldehyde modified carbon (MF-C) shifts positively by about 0.3 V (NHE) compared to the oxidized carbon, which does not contain nitrogen. The activity of catalysts for oxygen reduction further increases when the carbon was modified with thiourea formaldehyde (TUF), urea formaldehyde (UF), and selenourea formaldehyde (SeUF) resins, respectively.

Table 1
The amount of H_2O_2 produced at 0.5 V (NHE) during oxygen reduction on carbon-based catalysts modified with different nitrogen donors and heat-treated at 800 °C.

Nitrogen-modified carbon-based catalyst	% H_2O_2
MF-C	28
TUF-C	17
UF-C	3
SeUF-C	1

The onset potentials of oxygen reduction on these catalysts are approximately 0.7–0.8 V (NHE).

Fig. 3b shows the amount of H_2O_2 generated during oxygen reduction on carbon-based catalysts modified with different nitrogen donors and heat-treated at 800 °C. It is evident that the nitrogen modification significantly decrease the percentage of H_2O_2 produced during oxygen reduction in comparison with oxidized carbon.

Table 1 summarizes the amount of H_2O_2 produced at 0.5 V (NHE) during ORR on the carbon-based catalysts modified with different nitrogen donors. The amounts of H_2O_2 generated on MF-C and TUF-C at 0.5 V (NHE) are about 28% and 17%, respectively due to the presence of nitrogen groups. In the case of UF-C and SeUF-C, it further decreases to approximately 1–3% under our experiment conditions. These results indicated that the modification of nitrogen groups onto the oxidized carbon can greatly improves the activity and selectivity of carbon substrate towards oxygen reduction. Since UF-C and SeUF-C exhibited the optimum catalytic performances, the following study will be focused on these two samples.

Table 2 summarizes the BET surface areas of different samples: un-oxidized carbon, oxidized carbon, UF-C, and SeUF-C. The un-oxidized carbon has a surface area of 915 $m^2 g^{-1}$. After HNO_3 treatment, the surface area decreases to 694 $m^2 g^{-1}$ due to the destruction of micro- and meso-pores. After modification with nitrogen-containing polymer and subsequent heat-treatment, a further reduction in the surface area was observed for UF-C and SeUF-C. Moreover, the higher BET surface area of SeUF-C than that of UF-C may at least partially explain the slightly higher catalytic performance of SeUF-C compared to UF-C (see Fig. 3).

Fig. 4 shows the polarization curves of oxygen reduction on SeUF-C heat-treated at different temperatures. It can be seen that the activity of SeUF-C is strongly dependent on the heat-treatment temperature and the optimum temperature is 800 °C. The same tendency was also observed for UF-C.

Fig. 5a and b shows the XRD patterns of UF-C and SeUF-C before and after heat-treatment at 800 °C, respectively. The XRD patterns recorded before heat-treatment exhibit characteristic peaks corresponding to Se and/or UF in addition to a broad diffraction peak from carbon black. Upon heat-treatment, the diffraction peaks for carbon black become sharper indicating an increased graphitization. Moreover, only diffraction peaks from carbon were observed for heat-treated carbon-based catalysts. No any metal species was detected. TEM image shown in Fig. 6 further confirmed the absence of any metal in the catalytic structure. The ICP-MS analysis was carried out to analyze the bulk transition metals in UF-C and SeUF-C (see Table 3). A trace of transition metals was detected by University of Illinois at Urbana-Champaign.

Table 2
BET surface areas of different samples.

Sample	BET surface area ($m^2 g^{-1}$)
Un-oxidized carbon	915
Oxidized carbon	694
UF-C (heat-treated)	321
SeUF-C (heat-treated)	496

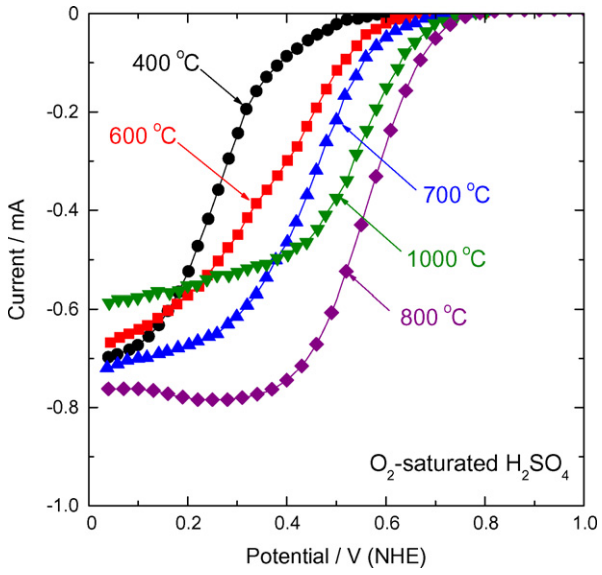

Fig. 4. Polarization curves of oxygen reduction on SeUF-C heat-treated at different temperatures between 400 and 1000 °C. The measurements were performed in O_2 saturated 0.5 M H_2SO_4 solution using a potential scan rate of 5 mV s^{-1} and a rotation speed of 900 rpm.

No metal impurities were observed for the same catalysts by Yonsei University. These results indicated that only nitrogen-modified carbon-based structures are responsible for the observed catalytic activity of UF-C and SeUF-C for oxygen reduction.

Fig. 7a shows the polarization curve of the H_2-O_2 PEM fuel cell prepared with the UF-C cathode catalyst (UF-C loading: 6.0 mg cm^{-2}). The testing was run at 75 °C with the H_2/O_2 back pressures of 30 and 40 psi, respectively. For comparison, the fuel cell performance prepared with 20 wt% Pt/C catalyst (Pt/C loading: 0.1 mg cm^{-2}) was also presented. The UF/C shows current density of 1.06 A cm^{-2} at 0.2 V; however, its performance is much lower than Pt/C counterpart. It is due to the lower intrinsic activity of UF-C for ORR in comparison with Pt/C. Another reason is that the large thickness of UF-C-based catalyst layer causes high electrical resistance and mass transfer resistance.

As shown in Fig. 7b, the thickness of UF-C-based catalyst layer with catalyst loading of 6 mg cm^{-2} is approximately 90 μm, while it is generally 3–5 μm for Pt/C-based catalyst layer with catalyst loading of 0.1 mg cm^{-2}. Fig. 7c shows the stability testing of UF-C catalyst at 0.4 V. The cathode catalyst loading is 4.0 mg cm^{-2}, and the H_2/O_2 back pressures are 30 and 30 psi, respectively. It can be seen that the UF-C-based fuel cell shows a stable current profile with current density of approximately 0.12 A cm^{-2} up to 200 h.

3.2. Discussion of nature of active sites of nitrogen-modified carbon-based catalysts

Table 4 provides the summary of surface composition of different samples determined by XPS. It was observed that the oxidized

Table 3
Bulk transition metal concentrations in UF-C and SeUF-C determined by ICP-MS.

Catalysts	Fe (wt%)	Co (wt%)
UF-C	0.00004[a]	0.00003[a]
	0[b]	0[b]
SeUF-C	0.00002[a]	0.000006[a]
	0[b]	0[b]

[a] Measured by University of Illinois at Urbana-Champaign.
[b] Measured by Yonsei University, Korea.

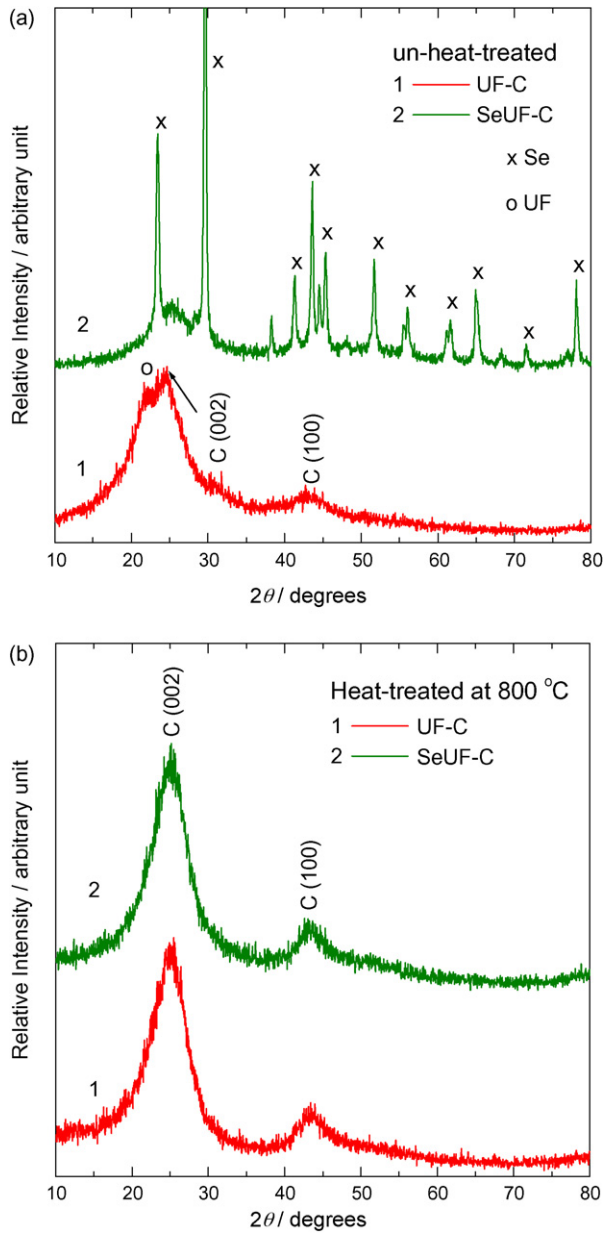

Fig. 5. XRD patterns of UF-C and SeUF-C (a) before and (b) after heat-treatment at 800 °C.

carbon has high oxygen concentration on the surface which was introduced by HNO_3 oxidation. After the polymerization on the oxidized carbon, the nitrogen concentration on the surface of carbon substrates increases. However, heat treatment at 800 °C can decrease the nitrogen concentration since the nitrogen can be partially removed in the form of small nitrogen-containing molecules at elevated temperature.

Table 4
Surface compositions of different samples determined by XPS.

Sample	Surface concentration (wt%)			
	C	N	O	Se
Oxidized carbon	95.0	–	5.0	–
UF-C (un-heat-treated)	88.2	8.4	3.4	–
UF-C (heat-treated)	92.4	2.2	5.4	–
SeUF-C (un-heat-treated)	89.6	5.8	3.5	1.1
SeUF-C (heat-treated)	92.3	2.4	5.1	0.2

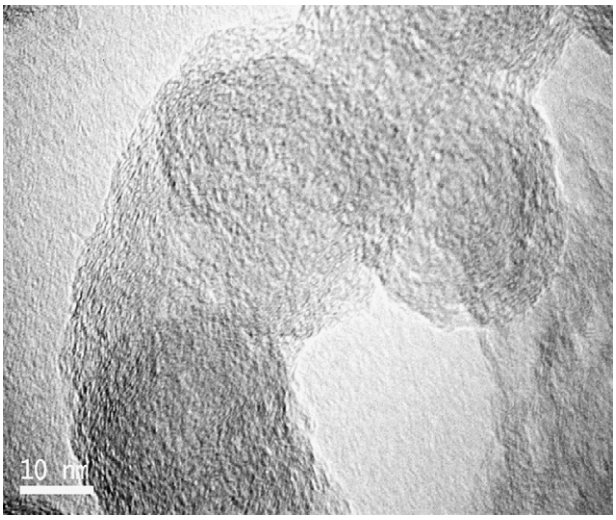

Fig. 6. TEM image of SeUF-C heat-treated at 800 °C.

XPS analysis was used to study the nature of nitrogen surface groups on the carbon support. The three common nitrogen groups observed in nitrogen containing carbonaceous materials are the pyridinic (ca. 398.6 eV), pyrrolic (ca. 400.3 eV) and graphitic nitrogen groups (ca. 401.1–403.6 eV) [46–48]. Pyridinic nitrogen refers to the nitrogen atom bonded to two carbon atoms on the edge of graphite planes that is capable of adsorbing molecular oxygen and its intermediates in oxygen reduction reaction. It has one lone pair of electrons in addition to the one electron donated to the conjugated π bond system, imparting Lewis basicity to the carbon [30]. Graphitic nitrogen, which is sometimes termed "quaternary" nitrogen, represents the nitrogen atom bonded to three carbon atoms within a graphite (basal) plane. Pyrrolic groups refer to nitrogen atoms that contribute to the π system with two *p*-electrons.

Fig. 8 shows the XPS spectra of N_{1s} region obtained for SeUF-C heat-treated at 600–1000 °C. The XPS spectrum for the catalyst heat-treated at 600 °C exhibits the three nitrogen groups, i.e., pyridinic, pyrrolic, and graphitic nitrogens. When the catalyst was heat-treated at 800 °C, the peak for the pyrrolic nitrogen is no longer observed from the XPS data. Increasing the heat-treatment temperature from 800 to 1000 °C transforms more of the pyridinic nitrogen to graphitic nitrogen. It should be noted that the sample heat-treated at 800 °C has larger fraction of the pyridinic nitrogen group compared to the pyrrolic and graphitic groups and it shows the highest activity. This indicated that the pyridinic nitrogen group is active for oxygen reduction and the catalyst heat-treated at 800 °C has more active sites (pyridinic nitrogen) to facilitate oxygen adsorption.

It is conceivable that the nitrogen atoms are attached onto the surface of the oxygen-rich (oxidized) carbon in the form of pyridinic and pyrrolic structures. During the subsequent heat-treatment step, carbon surface becomes richer in pyridinic nitrogen that enhances the activity of the catalyst for oxygen reduction. In the past, the general conception is that pyridinic nitrogen groups coordinated with a metal atom is responsible for the activity of non-precious metal catalysts. However, we observed that pyridinic N-rich carbon without metal is active for oxygen reduction since transition metal is not present on the surface of our catalysts.

According to Ref. [28,29], after heat-treatment at 800 °C in argon for Co-TMPP and Fe-TMPP, no Co or Fe was detected in the Mössbauer spectra in a form corresponding to coordination with nitrogen, thus indicating loss of the metal–N_4 centers. The macrocycle structure is rather completely destroyed after heat-treatment

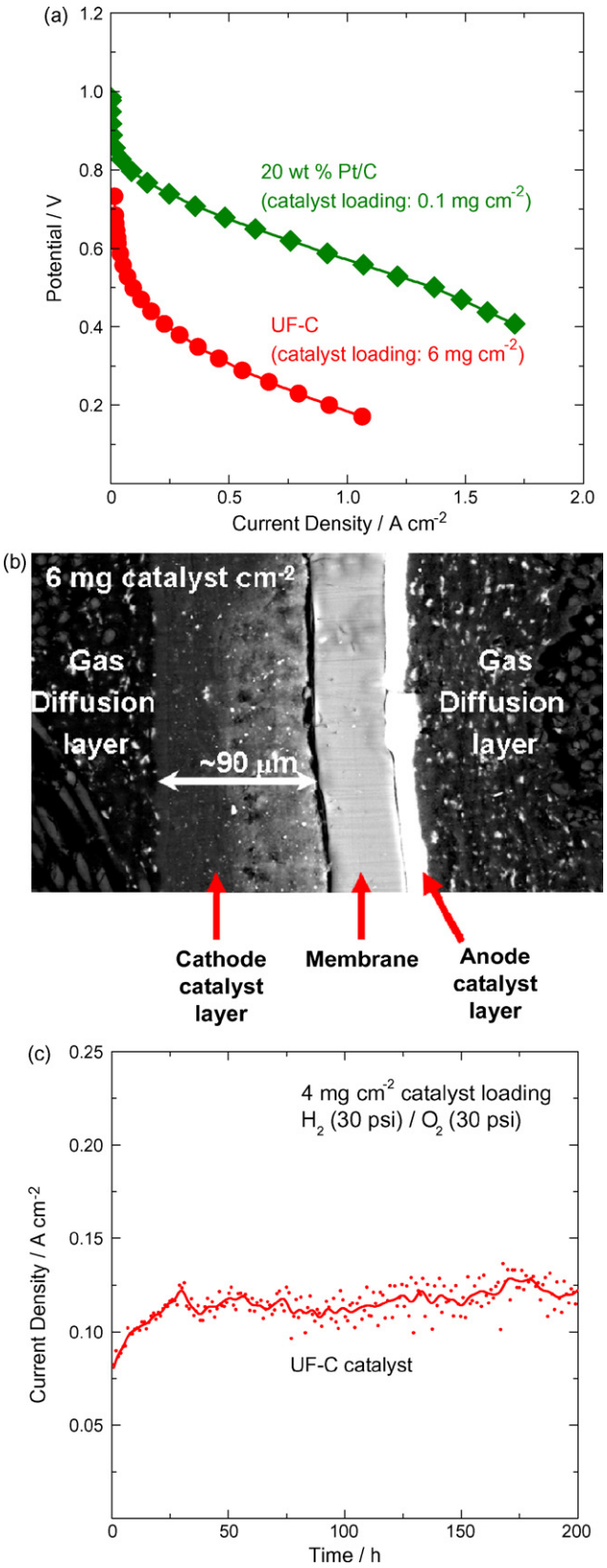

Fig. 7. (a) Polarization curve of the H_2–O_2 PEM fuel cells prepared with UF-C and 20 wt% Pt/C catalysts, respectively. UF-C loading: 6 mg cm^{-2}; Pt/C loading: 0.1 mg cm^{-2}; H_2/O_2 back pressures: 30 psi/40 psi; operation temperature: 75 °C. (b) SEM image of the cross-section of the MEA prepared with UF-C catalyst. (c) Current transient (stability test) at 0.4 V of the H_2-O_2 PEM fuel cell prepared with UF-C catalyst. Catalyst loading: 4 mg cm^{-2}; H_2/O_2 back pressures: 30 psi/30 psi; operation temperature: 75 °C.

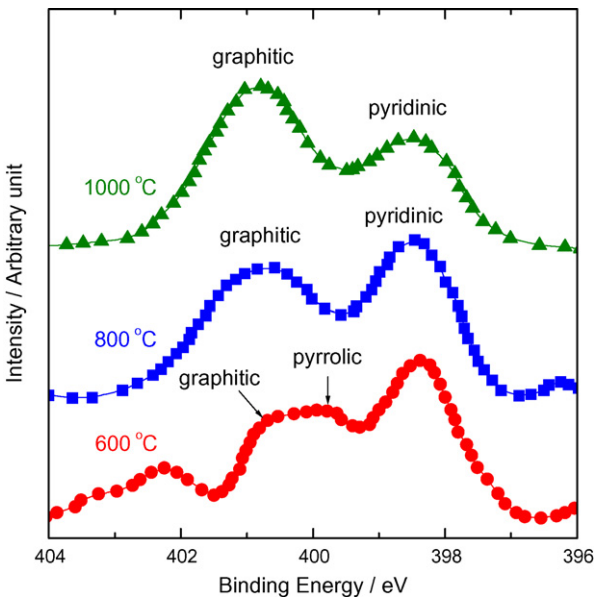

Fig. 8. XPS spectra of N 1s region obtained for SeUF-C heat-treated at 600–1000 °C.

at temperatures of 800–900 °C [49–51]. It was suggested that the transition metal does not act as an active site for oxygen reduction, but rather it serves primarily to facilitate the stable incorporation of nitrogen into the graphitic structure during high-temperature pyrolysis of metal–nitrogen complexes [28,29].

This has been strongly supported by our experimental findings on Co-based catalysts [37]. The XPS data indicated that the pyrolysis in the presence of Co increases the concentrations of two nitrogen functional groups on the carbon surfaces (pyridinic-type nitrogen and graphitic-type nitrogen), when compared with the case of the pyrolysis in the absence of Co. The subsequent dissolving out of Co metals from the heat-treated CoN chelate did not cause any loss of the catalytic activity; instead, the catalytic activity increased upon the chemical post-treatment for Co removal. From the extended X-ray absorption fine structures (EXAFS) study, we have also found that Co–N_4 chelates are not stable upon high-temperature pyrolysis above 800 °C.

Using a semi-empirical quantum chemical method, Strelko et al. [52] have shown that availability of 4–6% oxygen hetreoatoms of furan and pyrone-type and/or also 2–3% N of pyrol-type in a carbon matrix provide the greatest electron-donor ability to carbons. Two mechanisms of chemisorptions of oxygen on evacuated carbons were suggested namely: homolytic (free radical) at small degrees of filling of a surface by oxygen, and heterolytic (at large degrees of filling) causing the fixation of oxygen on a surface in the form of a superoxide ion O_{2-}^{*}.

According to Maldonado and Stevenson [30], on nitrogen doped carbon nanofiber electrodes, the oxygen reduction reaction can be treated as a catalytic regenerative process where the intermediate hydroperoxide (HO^{2-}) is chemically decomposed to regenerate oxygen. They have supported the proposed mechanism by electrochemical simulation and by measured difference in hydroperoxide decomposition rate constants. The results indicated that remarkable 100-fold enhancement for hydroperoxide decomposition for N-doped carbon nanofibers. The authors have concluded that exposed edge plane defects and nitrogen doping are important factors for influencing adsorption of reactive intermediates and for enhancing electrocatalysis for the oxygen reduction at nanostructured carbon electrodes. Our experimental studies indicate that a strong Lewis basicity of carbons doped with pyridinic and graphitic nitrogens facilitates the reductive adsorption reaction of O_2 with-

out the irreversible formation of oxygen functionalities, due to an increased electron-donor property of carbon.

4. Conclusions

This work showed that carbon-based catalysts for oxygen reduction can be synthesized by introducing oxygen and nitrogen groups from various nitrogen precursors. The nature of nitrogen surface groups and the effect of pyrolysis temperature on the activity of the catalyst have been evaluated. XPS indicated that high concentration of pyridinic type nitrogen groups doped on graphitic carbon increase the activity of catalysts. The carbon-based catalysts showed an onset potential at around 0.78 V (NHE) and the amount of H_2O_2 generated during oxygen reduction was approximately 1–3% at 0.5 V (NHE). On the carbon surface, pyridinic (quaternary) and graphitic nitrogens act as catalytic sites for oxygen reduction: particularly, pyridinic nitrogen, which possesses one lone pair of electrons in addition to the one electron donated to the conjugated π bond, facilitates the reductive oxygen adsorption and eliminates H_2O_2 formation.

Acknowledgement

The financial support of the Department of Energy (contract no. DE-FC36-03GO13108) is acknowledged gratefully.

References

[1] M.L. Rao, B.A. Damjanovic, J.O'.M. Bockris, J. Chem. Phys. 67 (1963) 2508.
[2] R.R. Adzic, in: J. Lipkowski, P. Ross (Eds.), Electrocatalysis, VCH Publishers, New York, 1998, pp. 197–242.
[3] N.M. Markovic, P.N. Ross, Electrochim. Acta 45 (2001) 4101.
[4] N.M. Markovic, P.N. Ross, Surf. Sci. Rep. 286 (2002) 1.
[5] H.A. Gasteiger, S.S. Kocha, B. Sompalli, F.T. Wagner, Appl. Catal. B 56 (2005) 9.
[6] R. Jasinski, Nature 201 (1964) 1212.
[7] A. Widelov, R. Larsson, Electrochim. Acta 37 (1992) 187.
[8] G. Lalander, R. Cote, D. Guay, J.P. Dodelet, L.T. Weng, P. Bertrand, Electrochim. Acta 42 (1997) 1379.
[9] R. Cote, G. Lalande, D. Guay, J.P. Dodelet, J. Electrochem. Soc. 145 (1998) 2411.
[10] P. Gouerec, M. Savy, J. Riga, Electrochim. Acta 43 (1998) 743.
[11] P. Gouerec, M. Savy, Electrochim. Acta 44 (1999) 2653.
[12] S.Lj. Gojkovic, S. Gupta, R.F. Savinell, Electrochim. Acta 45 (1999) 889.
[13] S.Lj. Gojkovic, S. Gupta, R.F. Savinell, J. Electroanal. Chem. 462 (1999) 63.
[14] M. Lefevre, J.P. Dodelet, P. Bertrand, J. Phys. Chem. B 104 (2000) 11238.
[15] H. Schulenburg, S. Stankov, V. Schunemann, J. Radnik, I. Dorbandt, S. Fiechter, P. Bogdanoff, H. Tributsch, J. Phys. Chem. B 107 (2003) 9034.
[16] S. Marcotte, D. Villers, N. Guillet, L. Roue, J.P. Dodelet, Electrochim. Acta 50 (2004) 179.
[17] K. Sawai, N. Suzuki, J. Electrochem. Soc. 151 (2004) A682.
[18] D. Villers, X. Jacques-Bedard, J.P. Dodelet, J. Electrochem. Soc. 151 (2004) A1507.
[19] K. Sawai, N. Suzuki, J. Electrochem. Soc. 151 (2004) A2132.
[20] S.-I. Yamazaki, Y. Yamada, T. Ioroi, N. Fujiwara, Z. Siroma, K. Yasuda, Y. Miyazaki, J. Electroanal. Chem. 576 (2005) 253.
[21] M. Yuasa, A. Yamaguchi, H. Itsuki, K. Tanaka, M. Yamamoto, K. Oyaizu, Chem. Mater. 17 (2005) 4278.
[22] F. Jaouen, F. Charreteur, J.P. Dodelet, J. Electrochem. Soc. 153 (2006) A689.
[23] R. Bashyam, P. Zelenay, Nature 443 (2006) 63.
[24] R. Yang, A. Bonakdarpour, E.B. Easton, J.R. Dahn, ECS Trans. 3 (2006) 221.
[25] E.B. Easton, A. Bonakdarpour, R. Yang, D.A. Stevens, D.G. O'Neill, G. Vernstrom, D.P. O'Brien, A.K. Schmoeckel, T.E. Wood, R.T. Atanasoski, J.R. Dahn, ECS Trans. 3 (2006) 241.
[26] J.-H. Kim, A. Ishihara, S. Mitsushima, N. Kamiya, K.-I. Ota, ECS Trans. 3 (2006) 255.
[27] T. Otsubo, S. Takase, Y. Shimizu, ECS Trans. 3 (2006) 263.
[28] E. Yeager, Electrochim. Acta 29 (1984) 1527.
[29] K. Wiesener, Electrochim. Acta 31 (1986) 1073.
[30] S. Maldonado, K.J. Stevenson, J. Phys. Chem. B 109 (2005) 4707.
[31] N.P. Subramanian, S.P. Kumaraguru, H.R. Colon-Mercado, H. Kim, B.N. Popov, T. Black, D.A. Chen, J. Power Sources 157 (2006) 56.
[32] B.N. Popov, DOE Hydrogen Program Annual Progress Report, V.C.2 (2006) 1–5.
[33] L. Liu, J.-W. Lee, B.N. Popov, J. Power Sources 162 (2006) 1099.
[34] L. Liu, H. Kim, J.-W. Lee, B.N. Popov, J. Electrochem. Soc. 154 (2007) A123.
[35] V. Nallathambi, G. Wu, N.P. Subramanian, S.P. Kumaraguru, J.-W. Lee, B.N. Popov, ECS Trans. 11 (2007) 241.
[36] X. Li, H.R. Colon-Mercado, G. Wu, J.-W. Lee, B.N. Popov, Electrochem. Solid-State Lett. 10 (2007) B201.
[37] V. Nallathambi, J.-W. Lee, S.P. Kumaraguru, G. Wu, B.N. Popov, J. Power Sources 183 (2008) 34–42.
[38] R.A. Sidik, A.B. Anderson, N.P. Subramanian, S.P. Kumaraguru, B.N. Popov, J. Phys. Chem. B 110 (2005) 1787.
[39] P.H. Matter, U.S. Ozkan, Catal. Lett. 109 (2006) 115.
[40] P.H. Matter, L. Zhang, U.S. Ozkan, J. Catal. 239 (2006) 83.
[41] P.H. Matter, E. Wang, J.-M.M. Millet, U.S. Ozkan, J. Phys. Chem. C 111 (2007)1444.
[42] A. Pizzi, in: A. Pizzi (Ed.), Wood Adhesives: Chemistry and Technology, Marcel Decker, New York, 1983.
[43] K. Kinoshita, J.A.S. Bett, Carbon 11 (1973) 403.
[44] H.P. Boehm, Carbon 32 (1994) 759.
[45] J.P. Chen, S. Wu, Langmuir 20 (2004) 2233.
[46] K. Stanczyk, R. Dziembaj, Z. Piwowarska, S. Witkowski, Carbon 33 (1995) 1383.
[47] R.J.J. Jansen, H. van Bekkum, Carbon 33 (1995) 1021.
[48] J. Casanovas, J.M. Ricart, J. Rubio, F. Illas, J.M. Jimenez-Mateos, J. Am. Chem. Soc. 118 (1996) 8071.
[49] V.S. Bagotzky, M. Tarasevich, K. Radysishkina, O. Levina, S. Andrisyova, J. Power Sources 2 (1977) 233.
[50] K. Wiesener, A. Fuhrmann, Z. Phys. Chem. 261 (1980) 411.
[51] A. Karsheva, S. Gamburtzev, I. Iliev, Elektrokhimiya 18 (1982) 127.
[52] V.V. Strelko, N.T. Kartel, I.N. Dukhno, V.S. Kuts, R.B. Clarkson, B.M. Odintsov, Surf. Sci. 548 (2004) 281.